

# Validation of electromagnetic field enhancement in near-infrared through Sierpinski fractal nanoantennas

Semih Cakmakyapan,<sup>1,2,\*</sup> Neval A. Cinel,<sup>2</sup> Atilla Ozgur Cakmak,<sup>3</sup>  
and Ekmel Ozbay<sup>1,2,4</sup>

<sup>1</sup>Department of Physics, Bilkent University, 06800 Ankara, Turkey

<sup>2</sup>Nanotechnology Research Center, Bilkent University, 06800 Ankara, Turkey

<sup>3</sup>Center for Nanotechnology Education and Utilization, The Pennsylvania State University, University Park, Pennsylvania 16802, USA

<sup>4</sup>Department of Electrical and Electronics Engineering, Bilkent University, 06800 Ankara, Turkey  
[semihc@bilkent.edu.tr](mailto:semihc@bilkent.edu.tr)

**Abstract:** We introduced fractal geometry to the conventional bowtie antennas. We experimentally and numerically showed that the resonance of the bowtie antennas goes to longer wavelengths, after each fractalization step, which is considered a tool to miniaturize the main bowtie structure. We also showed that the fractal geometry provides multiple hot spots on the surface, and it can be used as an efficient SERS substrate.

©2014 Optical Society of America

**OCIS codes:** (250.5403) Plasmonics; (220.4241) Nanostructure fabrication; (240.6695) Surface-enhanced Raman scattering.

---

## References and links

1. A. Kinkhabwala, Z. F. Yu, S. H. Fan, Y. Avlasevich, K. Mullen, and W. E. Moerner, "Large single-molecule fluorescence enhancements produced by a bowtie nanoantenna," *Nat. Photonics* **3**(11), 654–657 (2009).
2. B. J. Roxworthy, K. D. Ko, A. Kumar, K. H. Fung, E. K. Chow, G. L. Liu, N. X. Fang, and K. C. Toussaint, Jr., "Application of plasmonic bowtie nanoantenna arrays for optical trapping, stacking, and sorting," *Nano Lett.* **12**(2), 796–801 (2012).
3. P. J. Schuck, D. P. Fromm, A. Sundaramurthy, G. S. Kino, and W. E. Moerner, "Improving the mismatch between light and nanoscale objects with gold bowtie nanoantennas," *Phys. Rev. Lett.* **94**(1), 017402 (2005).
4. L. Wang and X. F. Xu, "High transmission nanoscale bowtie-shaped aperture probe for near-field optical imaging," *Appl. Phys. Lett.* **90**(26), 261105 (2007).
5. N. K. Emani, T. F. Chung, X. J. Ni, A. V. Kildishev, Y. P. Chen, and A. Boltasseva, "Electrically tunable damping of plasmonic resonances with graphene," *Nano Lett.* **12**(10), 5202–5206 (2012).
6. N. A. Hatab, C. H. Hsueh, A. L. Gaddis, S. T. Retterer, J. H. Li, G. Eres, Z. Zhang, and B. Gu, "Free-standing optical gold bowtie nanoantenna with variable gap size for enhanced Raman spectroscopy," *Nano Lett.* **10**(12), 4952–4955 (2010).
7. D. P. Fromm, A. Sundaramurthy, A. Kinkhabwala, P. J. Schuck, G. S. Kino, and W. E. Moerner, "Exploring the chemical enhancement for surface-enhanced Raman scattering with Au bowtie nanoantennas," *J. Chem. Phys.* **124**(6), 061101 (2006).
8. K. Kneipp, H. Kneipp, and J. Kneipp, "Surface-enhanced Raman scattering in local optical fields of silver and gold nanoaggregates-From single-molecule Raman spectroscopy to ultrasensitive probing in live cells," *Acc. Chem. Res.* **39**(7), 443–450 (2006).
9. H. Kneipp, J. Kneipp, and K. Kneipp, "Surface-enhanced Raman optical activity on adenine in silver colloidal solution," *Anal. Chem.* **78**(4), 1363–1366 (2006).
10. C. L. Haynes, A. D. McFarland, and R. P. Van Duyne, "Surface-enhanced Raman spectroscopy," *Anal. Chem.* **77**(17), 338A–346A (2005).
11. M. Moskovits, "Surface-enhanced spectroscopy," *Rev. Mod. Phys.* **57**(3), 783–826 (1985).
12. M. Kahl, E. Voges, S. Kostrewa, C. Viets, and W. Hill, "Periodically structured metallic substrates for SERS," *Sensor Actuat. Biol. Chem.* **51**, 285–291 (1998).
13. N. Guillot, H. Shen, B. Fremaux, O. Peron, E. Rinnert, T. Toury, and M. L. de la Chapelle, "Surface enhanced Raman scattering optimization of gold nanocylinder arrays: Influence of the localized surface plasmon resonance and excitation wavelength," *Appl. Phys. Lett.* **97**(2), 023113 (2010).
14. N. A. Cinel, S. Cakmakyapan, G. Ertas, and E. Ozbay, "Concentric ring structures as efficient SERS substrates," *IEEE JSTQE* **19**, 4601605 (2013).
15. N. A. Cinel, S. Bütün, G. Ertas, and E. Ozbay, "'Fairy Chimney'-shaped tandem metamaterials as double resonance SERS substrates," *Small* **9**(4), 531–537 (2013).
16. A. R. M. D. H. Werner, *Frontiers in Electromagnetics* (Wiley, 1999).

17. B. B. Mandelbrot and A. Blumen, "Fractal geometry - what is it, and what does it do," *P. Roy. Soc. Lond. A Mat.* **423**(1864), 3–16 (1989).
18. J. H. Zhu, A. Hoorfar, and N. Engheta, "Bandwidth, cross-polarization, and feed-point characteristics of matched Hilbert antennas," *IEEE Antenna Wireless Proceedings* **2**(1), 2–5 (2003).
19. V. Crnojevic-Bengin, V. Radonic, and B. Jokanovic, "Fractal geometries of complementary split-ring resonators," *IEEE T. Microwave Theory* **56**(10), 2312–2321 (2008).
20. D. H. Werner and S. Ganguly, "An overview of fractal antenna engineering research," *IEEE Antennas Propag.* **45**(1), 38–57 (2003).
21. G. Volpe, G. Volpe, and R. Quidant, "Fractal plasmonics: subdiffraction focusing and broadband spectral response by a Sierpinski nanocarpet," *Opt. Express* **19**(4), 3612–3618 (2011).
22. S. Sederberg and A. Y. Elezzabi, "Sierpinski fractal plasmonic antenna: a fractal abstraction of the plasmonic bowtie antenna," *Opt. Express* **19**(11), 10456–10461 (2011).
23. S. Sederberg and A. Y. Elezzabi, "The influence of Hausdorff dimension on plasmonic antennas with Pascal's triangle geometry," *Appl. Phys. Lett.* **98**(26), 261105 (2011).
24. P. Maraghechi and A. Y. Elezzabi, "Enhanced THz radiation emission from plasmonic complementary Sierpinski fractal emitters," *Opt. Express* **18**(26), 27336–27345 (2010).
25. L. Rosa, K. Sun, and S. Juodkazis, "Sierpinski fractal plasmonic nanoantennas," *Phys. Status Solidi-R* **5**(5-6), 175–177 (2011).
26. A. E. Krasnok, I. S. Maksymov, A. I. Denisyuk, P. A. Belov, A. E. Miroshnichenko, C. R. Simovski, and Y. S. Kivshar, "Optical nanoantennas," *Phys-Usp* **56**(6), 539–564 (2013).
27. J. S. Dahele and K. F. Lee, "On the resonant frequencies of the triangular patch antenna," *IEEE Trans. Antenn. Propag.* **35**(1), 100–101 (1987).
28. L. Novotny, "Effective wavelength scaling for optical antennas," *Phys. Rev. Lett.* **98**(26), 266802 (2007).
29. J. Anguera, C. Puente, C. Borja, R. Montero, and J. Soler, "Small and high-directivity bow-tie patch antenna based on the Sierpinski fractal," *Microw. Opt. Technol. Lett.* **31**(3), 239–241 (2001).
30. G. W. Bryant, F. J. Garcia de Abajo, and J. Aizpurua, "Mapping the plasmon resonances of metallic nanoantennas," *Nano Lett.* **8**(2), 631–636 (2008).
31. E. J. Smythe, E. Cubukcu, and F. Capasso, "Optical properties of surface plasmon resonances of coupled metallic nanorods," *Opt. Express* **15**(12), 7439–7447 (2007).
32. E. Prodan, C. Radloff, N. J. Halas, and P. Nordlander, "A hybridization model for the plasmon response of complex nanostructures," *Science* **302**(5644), 419–422 (2003).
33. N. Berkovitch and M. Orenstein, "Thin wire shortening of plasmonic nanoparticle dimers: The reason for red shifts," *Nano Lett.* **11**(5), 2079–2082 (2011).
34. K. D. Alexander, K. Skinner, S. P. Zhang, H. Wei, and R. Lopez, "Tunable SERS in gold nanorod dimers through strain control on an elastomeric substrate," *Nano Lett.* **10**(11), 4488–4493 (2010).
35. S. J. Lee, A. R. Morrill, and M. Moskovits, "Hot spots in silver nanowire bundles for surface-enhanced Raman spectroscopy," *J. Am. Chem. Soc.* **128**(7), 2200–2201 (2006).
36. S. M. Asiala and Z. D. Schultz, "Characterization of hotspots in a highly enhancing SERS substrate," *Analyst (Lond.)* **136**(21), 4472–4479 (2011).
37. K. H. Hsu, J. H. Back, K. H. Fung, P. M. Ferreira, M. Shim, and N. X. Fang, "SERS EM field enhancement study through fast Raman mapping of Sierpinski carpet arrays," *J. Raman Spectroscopy* **41**(10), 1124–1130 (2010).

---

## 1. Introduction

Optical bowtie antennas, which consist of two triangles separated by a gap, have been studied by many researchers over the years. Surface plasmon currents are excited on these nanoantennas and the induced charges are shared by the triangles that are capacitively coupled via the gap. In principle, they are similar to optical dipole antennas; but they can operate for larger bandwidths compared to dipole nanoantennas. This property provides flexibility in terms of the operation wavelength along with their scalable nature. Furthermore, the triangular features allow the excitation of higher order modes and the corners of the triangles generate lightning-rod effects that result in stronger field enhancement. Bowtie nanoantennas can be used in several applications, such as the enhancement of single-molecule fluorescence [1], single-particle trapping [2], measurement of optical intensity enhancements [3], integrated apertures for near-field optical imaging [4], tunable graphene nanophotonics devices [5], and Surface-enhanced Raman spectroscopy (SERS) owing to the strong electromagnetic field localization and enhancement [6]. It has also been shown that the bowtie antennas can be used as efficient SERS substrates [7]. SERS is a type of spectroscopy that provides vibrational information about the Raman-active analyte molecules adsorbed on roughened metallic surfaces. There are two fundamental mechanisms responsible for the enhanced Raman signal, which are electromagnetic [8, 9] and chemical enhancement mechanisms [10, 11]. The chemical mechanism, which results from the chemical binding of

the analyte molecules to the surface, is rather weak, when compared to the electromagnetic mechanism that is the dominant one. SERS benefits from the increased electric field due to the localized plasmons on nanostructured metallic surfaces. Controlling the SERS signal via patterned metallic nanostructures and arrays has been an attractive research area in recent years. There are several examples where the nanostructures with different geometries, shapes, and sizes have been used as SERS substrates [12–15]. As a rule of thumb, an optimal substrate should provide the highest possible average field enhancement at the metal molecule interface.

Euclidean abstractions may fall short in the representation of the structures in nature [16]. Many things in nature have similar appearances at different scales. Fractals can be employed in such cases. A fractal is a geometric shape that shows self-similar patterns [17]. It is impossible to implement a complete fractal physically and, therefore, the fractal growth should be halted at a certain growth stage. Strictly speaking, such geometries are called prefractals. However, the outcome of the fractal growths is almost always studied under the name fractals in the literature. We are also going to stick to the same terminology in the present paper. Fractals present multiperiodic structures that open up new operational bands in RF. Researchers have extensively studied fractal antennas to achieve improved performance by addressing the lacunarity, changing the fractal similarity dimensions ( $D_s$ ), antenna sizes and feed locations. Accordingly, fractal geometries have been used in applications such as miniaturized antennas [18], frequency-selective metamaterials [19], and multiband mobile telecommunication devices [20].

On the other hand, optical fractal antennas also received attention from researchers. It was theoretically shown that the fractal plasmonic antennas are advantageous in order to achieve a controlled broadband spectral response [21]. The same paper also numerically demonstrated that a Sierpiński nanocarpenter can be used to obtain a subdiffraction superfocusing within the vicinity of the nanoantenna surface. Another theoretical study pointed out that by designing plasmonic Sierpiński fractal bowtie antennas, it is possible to enhance the electric field within the gap, tune the spectral response at the near-infrared (NIR) wavelength regime, and red-shift the resonance wavelength after each iteration [22]. The influence of the Hausdorff dimension ( $D_s$ ) on the tunability of the Sierpiński nanoantenna was studied in another work [23], whereas a photoconductive THz emitter was proposed by utilizing complementary Sierpiński fractal geometries [24]. Rosa *et al.* considered a Sierpiński fractal plasmonic nanoantenna in [25], which would work by enhancing the extinction cross section in multiple bands. Nevertheless, to the best of our knowledge, a Sierpiński plasmonic nanoantenna has not been both numerically and experimentally investigated in NIR wavelengths so far, due to the plasmonic losses, difficulties in the fabrication and measurements [26].

In the current work, we have both experimentally and numerically demonstrated in NIR that the fractal bowtie nanoantennas operate at longer wavelengths after each fractalization compared to the conventional bowtie antennas of the same size. Moreover, they can further enhance the SERS efficiency due to the redistribution of the surface charges using conductively coupled subwavelength fractals, which also creates multiple electric field enhancement spots scattered over the fractal nanoantenna. Both the simulations and measurement results depict that as the degree of fractals is increased the SER signal intensity also increases.

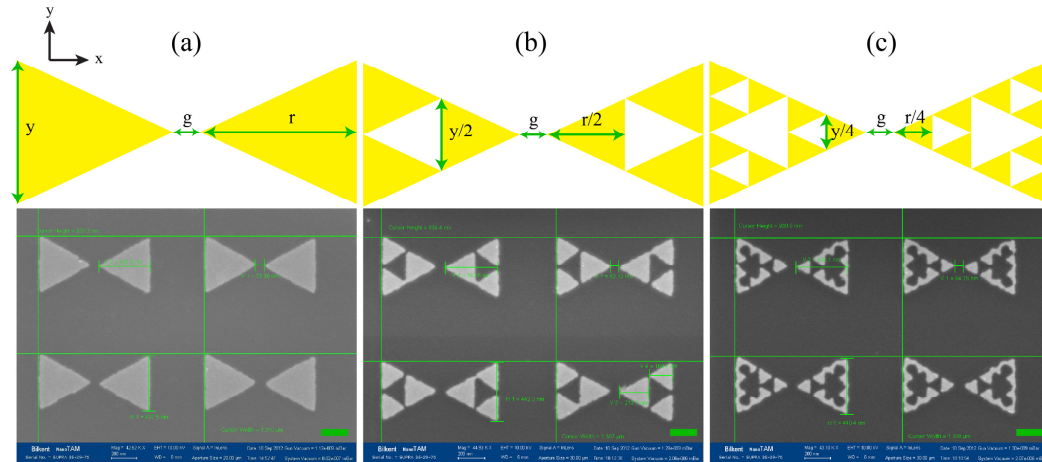


Fig. 1. Schematics (above) and SEM (below) images of (a) Bowtie, (b) Fractal-1, and (c) Fractal-2 structures.  $g = 65$  nm,  $r = 400$  nm,  $y = 420$  nm. Scale bar is 100 nm.

$$D_s = \frac{\ln 3}{\ln 2} \approx 1.585$$

## 2. Design and fabrication

Fractals are constructed by recursively using an operator on a basis shape. When the basis shape is a triangle, the resultant fractal is named a Sierpiński gasket (or Pascal's triangle modulo 2), and two tip to tip oriented equilateral Sierpiński triangles form a modified bowtie antenna. In this study, Fractal-1 is constructed by subtracting inverted triangles from the main bowtie antenna. The three equal triangles remaining on the structure after the subtraction are half the size of the original one. Fractal-2 is constructed by iterating the same procedure on the remaining triangles one more time. Schematics of the proposed structures are demonstrated in Fig. 1.

For the fabrication of the antennas, 300  $\mu\text{m}$  thick double-side polished sapphire substrate is cleaned and spin coated by 90 nm thick 950K A2 Poly(methylmethacrylate) PMMA, which is a positive-tone electron beam lithography resist. A water-soluble, conductive polymer called aquasave is spun on in order to prevent electrostatic charging. "Raith E-line Plus" electron beam lithography system is used for the exposure. The PMMA is exposed at 15 keV accelerating voltage using 10  $\mu\text{m}$  aperture size. After the exposure, the sample is developed with 1:3 MIBK:IPA solution for 40 seconds. Then, 5 nm titanium, as an adhesion layer, and 35 nm gold are deposited by using Leybold electron beam evaporator, followed by the standard lift-off process.

After fabrication, the physical dimensions and gap sizes of the resultant samples are measured by SEM. The gap size, height and base of the triangles are denoted by "g", "r" and "y", respectively in Fig. 1 where their dimensions are listed as  $g = 65$  nm,  $r = 400$  nm,  $y = 420$  nm. The total length of one antenna in x-direction for all these structures is  $g + 2r = 865$  nm, the size of the gap between the main triangles is  $g = 65$  nm, the periodicity in the x-direction is 1.3  $\mu\text{m}$ , and the periodicity in the y-direction is 930 nm. The dimensions are indicated in Fig. 1 for all the three shapes along with the SEM images of the antenna arrays.

## 3. Measurements

Transmission measurements are carried out using Vertex 70V FTIR Spectrometer with Hyperion 2000 IR Microscope. The sample is illuminated normally by a near-infrared (NIR) source with a  $\text{CaF}_2$  beam splitter and a polarizer. An InGaAs detector is placed inside Hyperion 2000 Microscope detector compartment in order to make measurements between the 800-2500 nm wavelength region.

For the SERS data collection Renishaw in Via Raman microscope equipped with a 785 nm laser is used. The laser power incident on the sample was 15 mW. The reported spectra are the average of 10 spectra collected with 10 ms acquisition times. 50x objectives, and 10 s accumulation time were standard for all of the samples. Benzenethiol was purchased from Sigma-Aldrich and used in the Raman experiments. The substrates for SERS experiments are prepared by spin coating benzenethiol (10 mM) solution in ethanol, at 4000 rpm for 40 seconds. This provided a homogeneous coating of the molecule all over the sensor surface [15].

#### 4. Simulations

A commercial software package, Lumerical FDTD Solutions, is used for the finite difference time domain (FDTD) simulations. The antenna arrays are modeled to be periodic perpendicular to the plane-wave propagation by using periodic boundary conditions, where the operating wavelength of the source is between 800 nm to 2500 nm. The boundary conditions in the illumination direction are set as perfectly matched layer (PML) to eliminate reflections from the boundaries. A spatial resolution of  $dx = dy = 1\text{ nm}$ ,  $dz = 2\text{ nm}$ , is chosen for an accurate calculation. The structures are illuminated by an x-polarized plane wave, which excites the antenna gap. The material data of gold are taken from Palik, and the sapphire substrate has a constant refractive index,  $n = 1.74$ , for the operating wavelength regime. The dimensions of the structures are in accordance with the physical sizes measured with SEM and are shown in Fig. 1. Small mesh size was necessary for more accurate calculations and for the investigation of electric field distributions on the surface of the antennas.

#### 5. Results and discussions

The transmission results of the antenna arrays are given in Fig. 2. Figure 2(a) shows the measurement results, and Fig. 2(b) shows the calculated transmission results. The results illustrate that the resonance wavelength of the main bowtie is around 1700 nm. On the contrary, the fundamental mode ( $TM_{1,0,-1}$ ) is expected to reside at around 1050 nm for an optical projection of the identical bowtie patch antenna with perfect electric conductor (PEC) triangles on a sapphire substrate [27]. PEC, as the name implies, perfectly reflects the impinging electromagnetic wave whereas real metals allow the penetration of the light which will interact with the oscillating free-electron gas and form surface plasmon polaritons. Hence, simulations with only theoretically available PECs help to appreciate the contribution of the plasmonic effects. Conversely, the scalability of Maxwell's equations permit the designers to roughly guess the length of the antenna for the corresponding operational wavelength. For example, a dipole antenna has an approximate total length ( $L$ )  $L \approx \lambda/2$  at the operational wavelength ( $\lambda$ ). This proportion holds very well till optical frequencies, as it is outlined in [28]. The scaling fails at these optical wavelengths due to the plasmonic effects and the resonance wavelength gets shifted to another value similar to the case we encounter for our structure. Moreover, the resonance wavelengths of Fractal 1 and Fractal 2 are 1900 nm and 2300 nm, respectively. While the structures are being miniaturized in each fractal case, the resonance wavelength is increasing. There is a good agreement between the transmission measurements and simulations. The differences mainly arise due to the fabrication imperfections, where the tips of the triangles are rounded, especially for Fractal-2.

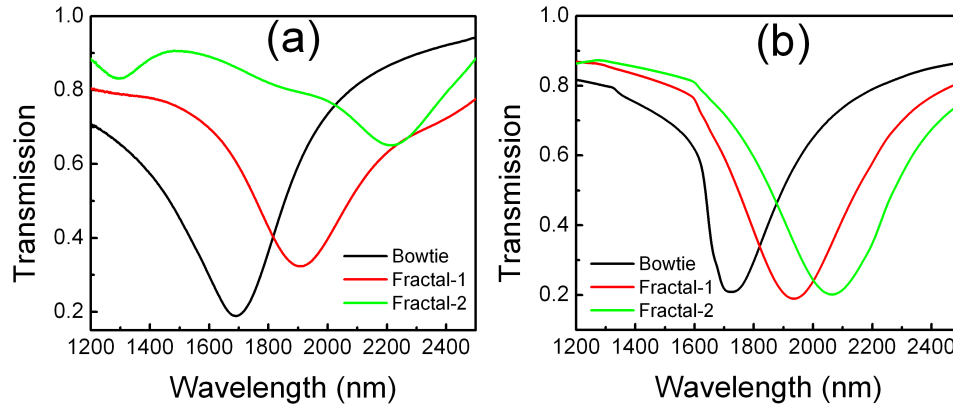


Fig. 2. Transmission spectra of the antenna arrays (a) experiment, (b) simulation results.

A similar resonance frequency shift of the fundamental mode toward longer wavelengths with fractalization is also observed at microwave frequencies for Sierpiński fractal antennas [29] and it has been well associated with an increase in the distributed self-inductance accompanied by the new perforations on the antenna [16]. Then, such shifts at optical wavelengths can also be automatically linked to the slight changes in impedance  $c$  as in the case of the microwave counterparts at first glance. However, further simulations (not shown here) have been carried out by replacing gold with PEC for the same nanoantennas in order to understand the contribution of the plasmonic effects. It is revealed that fractal nanoantennas with PEC parts produce only very minor shifts ( $\sim 10$  nm) with fractalization steps. Therefore, the shifts at optical wavelengths with real metals should be dominantly attributed to the modifications on the surface plasmon currents of the nanoantennas. If the shifts were mainly caused by the additional self-inductances coming from the perforations, we would end up seeing pronounced resonance wavelength shifts while still assigning PEC as the building block of the fractal nanoantennas. The elucidation of this phenomenon can be helpful in understanding the working principles of such antennas.

The bowtie antenna comprises two triangles that constitute coupled dipole moments. We can only excite the x-polarized modes (bright modes) along the polarization direction of the incident plane wave in our current configuration. This effective coupling between the triangles already causes red shifts from the original resonance frequency of the individual triangles for the bright modes. Hence, an additional red/blue shift is well known to be a consequence of an increase/decrease in the dimension of the nanoantenna along the axis of the polarization [30] or a decrease/increase in the size of the gap in between the triangles [31]. Fractalization takes out certain portions of the metal and creates nanocavities. Generally, nanocavities hybridize the supported plasmonic modes and generate bonding and antibonding states with slightly altered frequencies depending on the strength of the interaction between the cavity and outer layer plasmons [32]. In case of a bonding state, the plasmon mode can be tuned to longer wavelengths by decreasing the thickness of the surrounding metallic frame, which dictates extracting out larger portions of the metallic layer from the original bowtie. Another scenario for coupling can be visualized between the connected subwavelength features; triangles in our case. The touching spots of the triangles enables a bridge to redistribute the surface charges in a delocalized fashion, as suggested in [33]. The near-field interactions compel both of these coupling scenarios to come into play for higher modes at shorter wavelengths, too. The fractalization stages alter the polarizability as well as the extinction spectra of the bowtie nanoantenna. As a result, in certain wavelength regimes the fields tend to get scattered over the Sierpiński fractal nanoantennas rather than getting localized just in the vicinity of the gap or along the equilateral outer side walls. Moreover, the number of the intensified electrical field points on the surface of the Sierpiński fractal

nanoantennas is boosted while the surface charges get delocalized. These changes are the results of the plasmonic coupling between the subwavelength features.

The ideal fractal parts of the Sierpiński fractal antennas touch each other at a single point. However, each triangle element needs to be connected to its neighboring triangle in the simulations in order to avoid the geometric singularities [22]. Otherwise, a collective excitation from all of the triangles cannot be obtained due to the discontinuity. We showed in Fig. 3(a) that the connection of the triangles is very crucial. The fractal resonance completely deteriorates if the triangle elements are separate from each other. Moreover, a rather weak resonance is measured at smaller wavelengths, which originates from the individual triangles. In other words, the configuration acts such as a triangular plasmonic array. FDTD simulations are carried out in order to validate this deduction. For that case, the configuration acts as a set of capacitively coupled single subwavelength triangles and yields a weak resonance at 1200 nm when the triangles are isolated. From the framework of the plasmonic coupling discussions that are outlined in the previous paragraph, the red-shifted resonance at 1900 nm is the result of the hybridization and conductive coupling effects. It is seen in Fig. 3(b) that the resonance dip of the Fractal-1 is achieved when the tips of the neighboring triangles are touching. Therefore, it is important that the fractals are connected for the continuum of the current density.

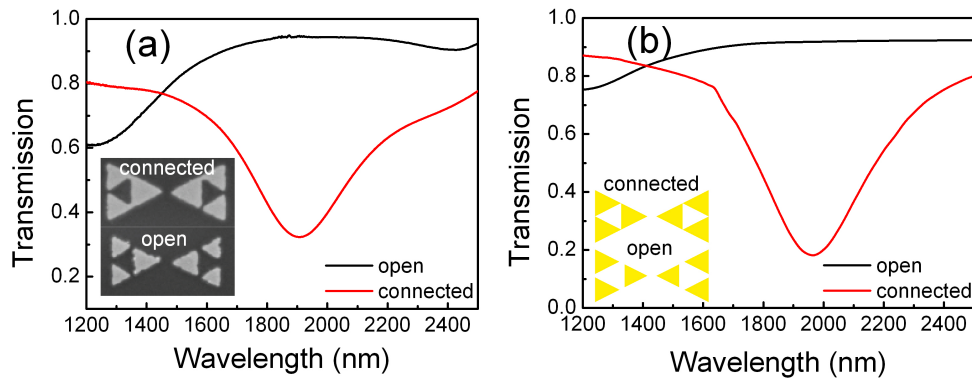


Fig. 3. Transmission spectra of open and connected Fractal-1 structures: (a) experiment, (b) simulation.

The fractal bowtie nanoantennas are expected to exhibit an extraordinary enhancement and electric field localization when compared to the conventional bowtie antenna. This is due to the increased density of the hotspots generated in the cavities for both designs, which in turn excites a larger area on the metal surface, even though the area of the metal is decreased after each fractalization. The enhanced localized fields on the fractal antennas provide a platform as efficient SERS substrates. It has been shown before that the higher the density of hot-spots, the higher the total signal intensity in SERS will be [7, 34–36]. Raman measurements of the structures are given in Fig. 4. SERS signal intensity at  $1075\text{ cm}^{-1}$  is enhanced by a factor of 8 for Fractal-1, and it is enhanced 16 times for Fractal-2 when compared to the conventional bowtie antenna.

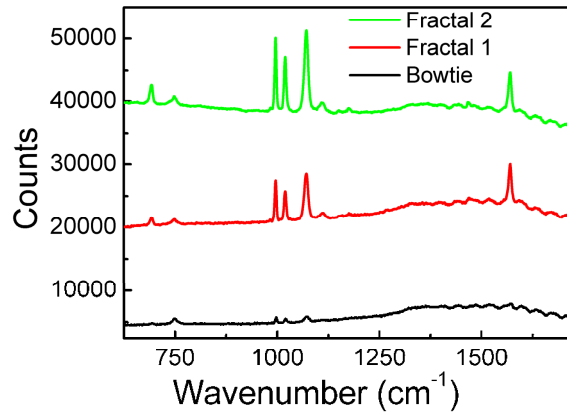


Fig. 4. SERS measurement results for Bowtie, Fractal-1 and Fractal-2.

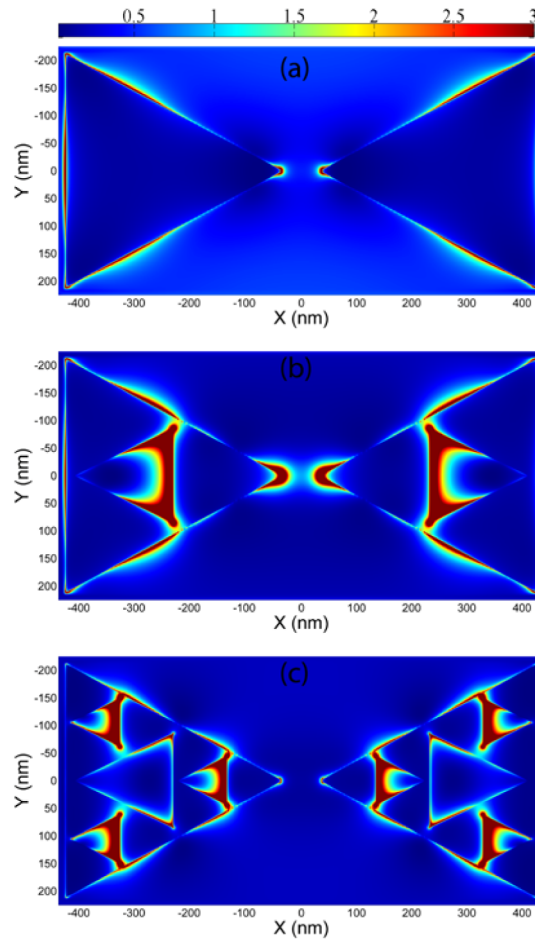


Fig. 5. Electric field distributions at the Stokes shifted wavelength, 895 nm. (a) Bowtie, (b) Fractal-1, and (c) Fractal-2. The maximum of the color bar is set to the same value for comparison.

Figure 5 shows the electric field distribution of bowtie, Fractal-1, and Fractal-2 structures at 895 nm, which is the Stokes shifted wavelength. In Fractal-1, the simulations show a higher electric field distribution both in the cavity and in between the tips of the triangles forming the bowtie. Moreover, for the case of Fractal-2 geometry, this is further enhanced since the number of engravings that serve as hotspots is increased. The figures clearly depict that the hot spots responsible for the surface enhanced Raman effect are becoming more dominant as the degree of fractals is increased.

In [37], Hsu et al has shown SERS enhancement with a Sierpiński carpet for which the isolated nanostructures contributed to the electric field localization. Higher electric field enhancement values can be attained in comparison to the continuous metal films. The enhanced SERS factors rely on localized surface plasmons rather than surface plasmons in such structures. On the other hand, the conductive bridges between the self-similar triangles are vital to generating again self-similar electric field distributions as shown in Fig. 5 for the Sierpiński fractal bowtie nanoantennas.

The electric field distribution is obtained for all three designs both at the excitation and Stokes shifted wavelengths. Then,  $|E_{Excitation}|^2 \cdot |E_{Stokes}|^2$  is integrated over the gold areas. According to the simulation results, the integrated E-field is 24 times the bowtie antenna for Fractal-1, and 32 times the bowtie antenna for Fractal 2.

## 5. Conclusion

In conclusion, we experimentally and numerically demonstrated that the fractal bowtie antennas operate at longer wavelengths compared to the conventional bowtie antenna of the same size, even though the metallic area is reduced after each fractalization. Furthermore, we showed that the fractal antennas have multiple hot spots, in which the electric field is enhanced and localized. We measured that these hot spots increase the SERS signal. The experimental results and the simulations showed good agreement. It is possible to use such structures as frequency-selective miniaturized antennas, and efficient SERS substrates.

## Acknowledgment

This work is supported by the projects DPT-HAMIT, DPT-FOTON, NATO-SET-193 and TUBITAK under Project Nos., 113E331, 109A015, 109E301. One of the authors (E.O.) also acknowledges partial support from the Turkish Academy of Sciences. The authors express their thanks to Koç University, Surface Science and Technology Center for the Raman system and Assistant. Prof. Dr. Uğur Ünal and Dr. M. Barış Yağcı for their technical assistance in the Raman measurements.